Available online at www.sciencedirect.com
SCIENCE DIRECT
Polymer 47 (2006) 5897–5908
polymer
www.elsevier.com/locate/polymer

Physical and mechanical characterization of oriented polyoxymethylene produced by die-drawing and hydrostatic extrusion

J. Mohanraj [a], M.J. Bonner [b], D.C. Barton [a], I.M. Ward [b,*]

[a] School of Mechanical Engineering, University of Leeds, Leeds LS2 9JT, UK
[b] School of Physics and Astronomy, University of Leeds, Leeds LS2 9JT, UK

Received 10 February 2006; accepted 28 May 2006
Available online 23 June 2006

Abstract

The mechanical properties and structure of uniaxially oriented polyoxymethylene (POM) produced by two solid-state processes, hydrostatic extrusion and die-drawing, are compared. In the former process there is no net component of tensile stress whereas in the latter case the sample is subjected to axial tensile stresses at the die-exit. The tensile nature of the stresses in die-drawing causes void formation and growth in the oriented sample whereas, in the case of hydrostatic extrusion, voids are suppressed due to the compressive stress fields. The mechanical properties of the oriented samples are compared together with relevant structural data, and their differences discussed.

Keywords: Polyoxymethylene; Orientation; Mechanical properties

1. Introduction

Substantial improvement in properties as a result of molecular orientation has initiated the development of several solid-state forming processes to orient semi-crystalline and amorphous polymers [1–6]. The changes in the microstructure and the associated enhancement in the mechanical properties on orientation have also led to many scientific and theoretical attempts to understand the relationships between the properties and the structure of the oriented materials. Despite the progress made to achieve property enhancement in solid-state oriented polymer products on a laboratory scale, the commercial viability of the processes has often been restricted due to the apparent limitation of the production speed.

In hydrostatic extrusion, where the deformation takes place with no net tensile stress, the flow stress increases due to strain hardening at high degrees of plastic strain and also due to the effect of the hydrostatic component of stress. Increasing the extrusion pressure is then counter productive and the flow stress rises to the point where the extrusion rate is negligible and in practical terms no further increase in pressure is beneficial. In die-drawing, the hydrostatic component of stress is small and the flow stress increases due to strain hardening and strain rate sensitivity to a point where it exceeds the fracture strength of the drawn oriented polymer. Hence fracture occurs as higher speeds are attempted.

Structural defects such as micro-voids or inter-lamellar voids, of few nanometers in size, when present in a polymer are thought to act as potential failure sites when the polymer is deformed in tension. This premature fracture could limit the potential of the polymer in commercial applications such as solid-state wire drawing where high drawing speed and enhanced mechanical properties are of prime importance.

In this paper the focus will be on polyoxymethylene (POM). POM is an engineering semi-crystalline thermoplastic polymer, which in its oriented form combines the properties of high axial strength and stiffness [4,7–9]. Oriented POM has also been shown to exhibit superior resistance to creep [10], low coefficient of thermal expansion [11], heat shrinkage [12] and has been found to possess good chemical and weather

* Corresponding author. Tel.: +44 113 3433808; fax: +44 113 3433846.
E-mail address: i.m.ward@leeds.ac.uk (I.M. Ward).

0032-3861/$ - see front matter © 2006 Elsevier Ltd. All rights reserved.
doi:10.1016/j.polymer.2006.05.056

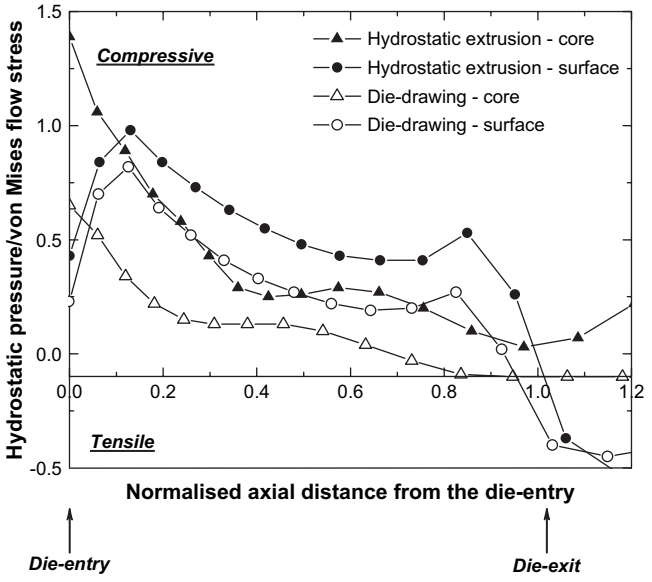

Fig. 1. Hydrostatic pressure/von Mises flow stress vs. the normalized axial distance from the die-entry for the hydrostatic extrusion and die-drawing processes.

resistance [13]. However, past research on POM has shown that this polymer when subjected to tensile deformation is very much susceptible to structural defects such as voids [4,14,15].

In the present paper the properties of oriented POM produced by two solid-state orientation processes, die-drawing and hydrostatic extrusion, are compared. In die-drawing, the sample is subjected to an axial tensile stress at the die-exit whereas in hydrostatic extrusion there is no net tensile stress during deformation.

The stress state of the material in the die for both the processes can be analyzed with the aid of finite element simulations. Details of the finite element model have been published elsewhere [16]. Fig. 1 shows the state of stress, defined as the ratio of the hydrostatic pressure, P, to the von Mises flow stress, Y, at the core and surface of the sample as it progresses through the die for a nominal draw ratio of 2 and 10° semi-die angle. The normalized distance of 0 and 1 indicates die-entry and exit, respectively. For the hydrostatic extrusion process, the stress state in the core and surface of the material in the die is compressive whereas for the die-drawing process the stress state in the material at the core and the surface is initially compressive and becomes tensile at about 70–80% of the die length into the die. The aim of the present work is to analyze the effect of the stress state on the subsequent structural, mechanical and physical properties of the oriented products.

2. Experimental

2.1. Materials

The material used in this study was Delrin® 7031 supplied by DuPont (UK) Limited, Hertfordshire. The density, number average molecular weight and polydispersity of this grade of POM were 1.423 g/cm^3, 66 000 and 2, respectively. The melt temperature and %crystallinity of this grade, determined by DSC at a scanning rate of 10 °C/min, were 178 ± 1 °C and $62 \pm 0.5\%$, respectively.

For both hydrostatic extrusion and die-drawing, POM rods of 20 mm diameter were extruded at 200 °C and cut to 1 m lengths. On each rod, a conical tag of diameter equal to that of the die-exit with a taper of semi-angle identical to that of the die was machined to aid the start-up procedure for the hydrostatic extrusion and die-drawing processes. In the case of the hydrostatic extrusion process, all the dies used for the present work were conical with a semi-angle of 15°. For die-drawing, the semi-angle of the conical dies was 10°. In both processes, the die-exit was characterized in terms of the nominal draw ratio, R_N, defined as the ratio of the cross-sectional area of the billet to the cross-sectional area at the die-exit. The total degree of deformation experienced by the material was expressed by the actual draw ratio, R_A, which was defined as the ratio of the initial and final cross-sectional areas of the billet.

2.2. Hydrostatic extrusion

A schematic sketch of the hydrostatic extrusion facility is shown in Fig. 2. In this process, the billet was forced through the die by the pressurized hydraulic fluid. The fluid used in the present work was castor oil as recommended for short-term POM extrusions [10]. The hydrostatic extrusion tooling was contained within the pressure vessel that was heated independently by three band heaters. Because of the high operating temperatures and pressures in the pressure vessel, O-rings and anti-extrusion brass rings were used between the die and die holder to give a good pressure seal.

In a typical extrusion run, the billet was loaded into the pressure vessel and the vessel was filled with oil. The band heaters, controlled by independent Eurotherm temperature controllers, were switched on to achieve the desired temperature as measured by thermocouples situated close to the inner surface of the pressure vessel. A small pressure of about 7 MPa was maintained inside the pressure vessel during the heating stage to push the billet against the die walls. The rise in pressure inside the vessel due to thermal expansion of the oil during the heating stage was vented by releasing the relief valve. A small axial force was applied to the end of the polymer tag by means of a pulley and a dead weight system to keep the product straight. A potentiometer was fixed to the cable near the pulley to monitor the displacement of the extruded product. The signal from the potentiometer was monitored during the extrusion cycle to indicate the end of the process when the desired length of polymer had been extruded. After achieving the desired temperature in the billet, the pressure was gradually increased in the vessel by the movement of the piston. Once the tag had emerged out of the die, the extrusion was performed at constant pressure to keep the extrusion rate constant at around 2 mm/min. At the end of the extrusion run, the heaters were switched off and the pressure in the vessel was released gradually by easing the pressure valve. Once

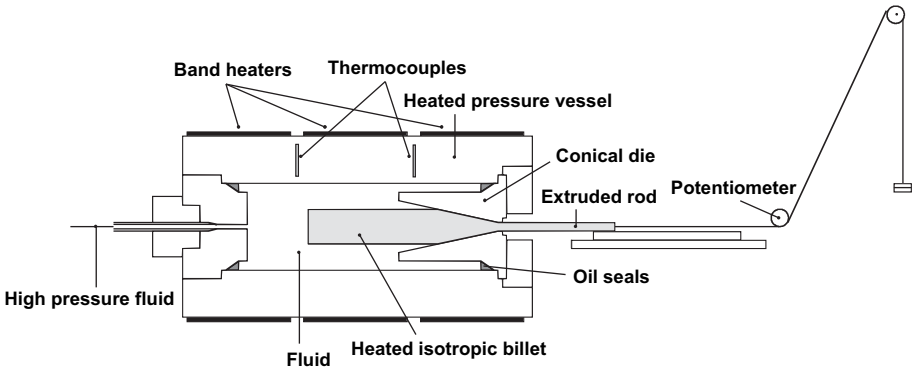

Fig. 2. Schematic of the hydrostatic extrusion process.

the assembly had cooled to about 50 °C, the die assembly was ejected by applying air pressure of 0.5 MPa and the product was cut-off. In the present study, POM billets were drawn at 160 °C and different pressures to different actual draw ratios (R_A) up to 10. The maximum achievable draw ratio was limited by the capacity of the pressure intensifier, which was 500 MPa.

2.3. Die-drawing

The die-drawing machine is shown schematically in Fig. 3. It consisted of three heating chambers heated by independent Eurotherm temperature controllers. The die was mounted onto a die holder and located on a revolving frame, which enabled the sample to be rotated during the heating stage to ensure thermal equilibrium through the cross-section of the billet. The temperature of the die holder was maintained at the draw temperature, independently from the heating chamber, by a Eurotherm with the thermocouple positioned close to the working surface of the die. The haul-off was provided by a chain, driven by an electric motor through a gearbox unit. Variable haul-off speeds ranging from 50 mm/min to about 15 m/min can be achieved by adjusting the controller. A load cell was attached to the haul-off carriage and the drawing load was displayed on a digital meter during the run.

The billet was placed in the heated chamber maintained at 160 °C and the tag gripped by the haul-off unit. The material was allowed to soak at the draw temperature for 90 min to establish thermal equilibrium. After the soaking period, the tag was drawn at a slow speed of 5 mm/min until the oriented material emerged. At this point the drawing process was stopped and restarted with the product now re-gripped by the haul-off unit. All the samples were drawn at a slow speed of 5 mm/min to minimize the free drawing outside the die and to match the output speed in the hydrostatic extrusion process. After the drawing experiment, the product and the billet remaining in the die were cooled under load before being removed from the machine. The diameter of the product was measured while the product was still under load. In the present study, different draw ratios were achieved by either changing the diameter of the billet or that of the die-exit.

2.4. Structural characterization

For structural studies on the isotropic and oriented POM, a rectangular strip of thickness 2 mm was machined in the transverse direction from the core of the cylindrical rods. The incident X-ray beam in both WAXS and SAXS measurements was perpendicular to the axial (draw) direction.

2.4.1. WAXS

The WAXS studies on the isotropic and oriented POM samples were performed using a Siemens X-ray machine with Cu Kα radiation of wavelength $\lambda = 1.542$ Å generated at 40 kV and 30 mA. The 2θ scans were determined in a Huber texture goniometer in reflection geometry in the angular range of 15–35° in steps of 0.04°. The crystalline orientation function was determined by an azimuthal scan of the (100) plane from 0° to 90° in steps of 0.2°. The Huber was controlled by HUTEX software in a Hewlett Packard Vectra ES/12 computer.

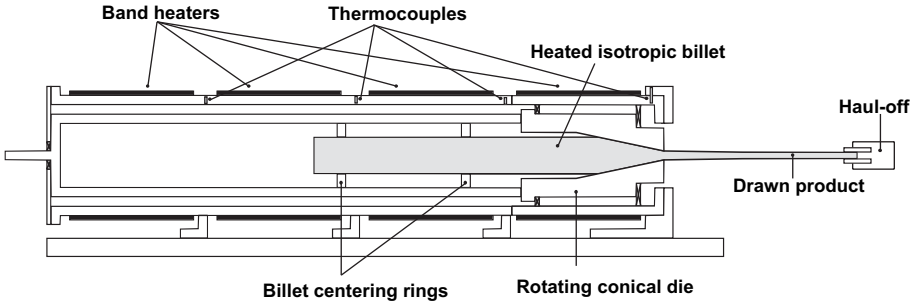

Fig. 3. Schematic of the die-drawing process.

2.4.2. SAXS

Small-angle X-ray scattering (SAXS) patterns were obtained using the Siemens small-angle diffractometer. The Cu Kα radiation of wavelength $\lambda = 1.542$ Å generated at 40 kV and 30 mA was collimated to a diameter of 0.7 mm. The SAXS patterns were collected using a Siemens Hi-Star 2-dimensional area detector for 5 min at 20 °C under vacuum. The detector to sample distance was fixed at 420 mm with the beam stop positioned halfway between the sample and the detector. After each scan, a background pattern was collected without the sample for the same duration and subtracted from the sample pattern.

2.5. Thermal characterization

The thermal characterization of the isotropic and oriented POM samples was carried out using a Perkin Elmer DSC-7 analyser. The melting temperature was determined at a heating rate of 10 °C/min using a sample weight of 5 mg under nitrogen atmosphere. The calibration of the temperature and enthalpy of the system was carried out using indium. The results reported are an average from 5 scans.

2.6. SEM

SEM was used to provide information on the damage in the oriented material. Samples for SEM were taken from the central section of the oriented rods transverse to the axial (draw) direction. The surface of the samples was cut using a sledge microtome. After micro-toming the samples were heated to 35 °C to relieve any residual stresses induced during the micro-toming process. Using a cotton swab, the surface of the samples was exposed to the vapour of hexa-fluoro-propanol to open any cavities that might have closed during the micro-toming process. The samples were then coated with gold using an Emscope SC500 SEM coating unit. The SEM micrographs were taken using a Philips XL30 ESEM operated in the secondary electron mode at a 20 kV accelerating voltage. Micrographs were taken parallel to the draw direction.

2.7. Density

The density of the isotropic and drawn samples was obtained from the mass per unit volume.

2.8. Tensile tests

Cylindrical dumbbell samples of gauge length 30 mm and diameter 3 mm were machined from the isotropic and oriented rods. In the case of the oriented rods, the axis of the sample was parallel to the orientation direction. The sample ends were loaded in 'V' shaped serrated grips and tested at 20 °C at a crosshead speed of 1 mm/min in an Instron universal tensile testing machine. The load–displacement plot was saved on a computer for later analysis. The modulus was determined from the initial load–displacement curve using a video extensometer attached to the testing machine. The strength was determined by dividing the peak load in the load–displacement plot by the initial cross-sectional area of the sample. At each draw ratio, at least 6 samples were tested and the average values of the modulus and strength were calculated.

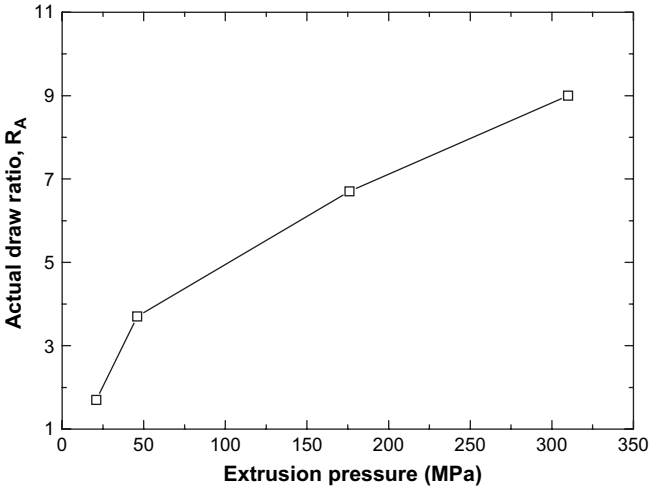

Fig. 4. Relationship between the actual draw ratio and extrusion pressure for the hydrostatic extrusion process.

3. Results and discussion

3.1. Hydrostatic extrusion process

The relationship between extrusion pressure and the final actual draw ratio (R_A) is shown in Fig. 4. The draw ratio does not increase linearly with extrusion pressure; instead it increases sharply for draw ratios less than 4 and then rises gradually for higher draw ratios. Similar behaviour has been observed for linear polyethylene [17], a different grade of polyoxymethylene [10] and glass fibre filled POM [18]. Hope and Ward [19] explained the rise in the extrusion pressure with draw ratio in the hydrostatic extrusion process using an

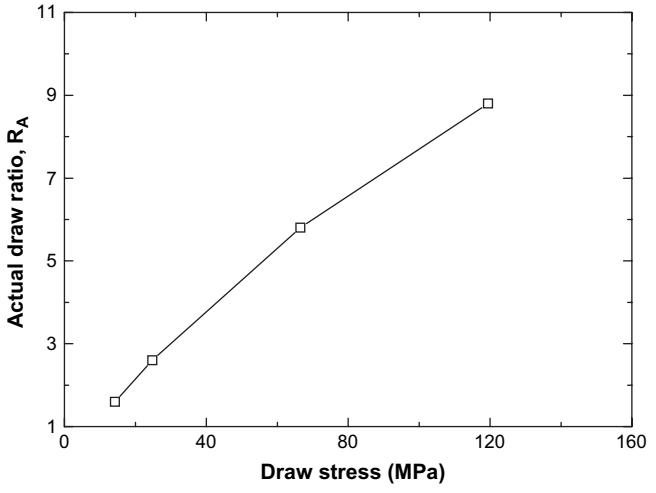

Fig. 5. The variation of actual draw ratio with draw stress for the die-drawing process.

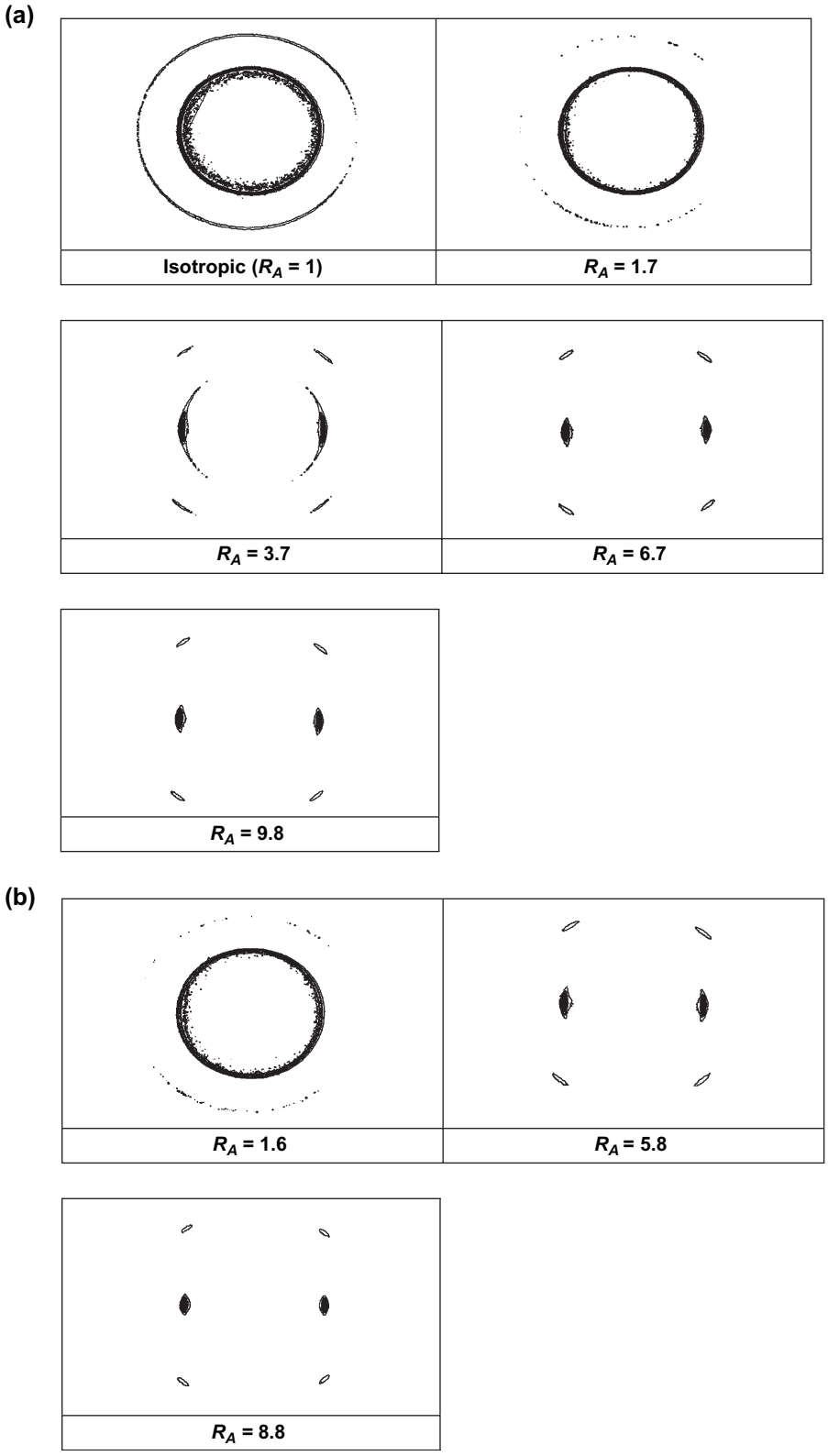

Fig. 6. WAXS patterns at different draw ratios for (a) hydrostatically extruded and (b) die-drawn samples.

activated rate theory approach. They argued that the upward curvature in the extrusion pressure for draw ratio greater than 4 is due to the combined effects of strain, strain rate and pressure on the flow stress and the billet–die friction.

3.2. Die-drawing process

The variation of draw stress with actual draw ratio (R_A) for the die-drawing process is shown in Fig. 5. The draw stress

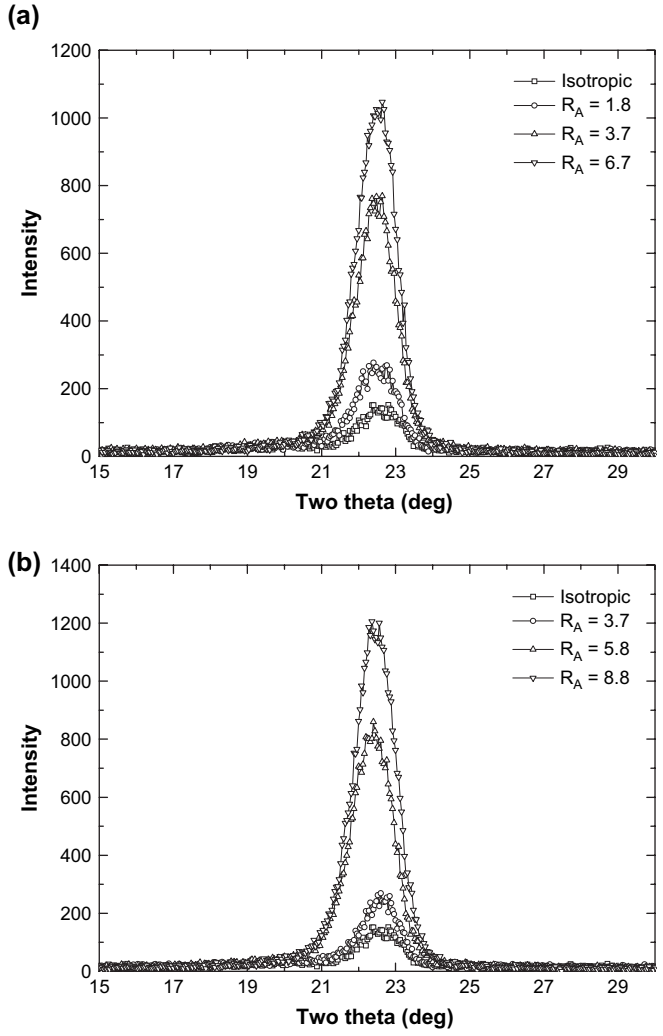

Fig. 7. X-ray intensity from the (100) plane measured as a function of 2θ at different draw ratios for (a) hydrostatically extruded and (b) die-drawn samples.

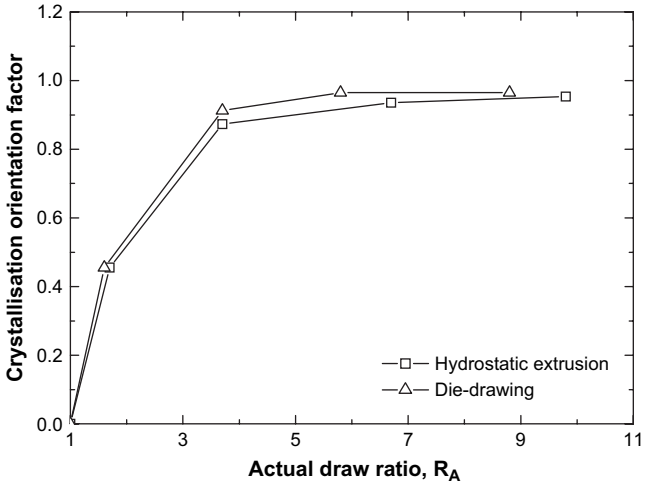

Fig. 8. The crystalline orientation factor as a function of draw ratio for hydrostatically extruded and die-drawn POM.

was based on the drawing load measured by means of a strain-gauged load-cell mounted on the haul-off carriage and the product cross-sectional area. In general, for a fixed drawing speed, the drawing stress increased linearly with actual draw ratio irrespective of the nominal draw ratio of the die. This suggests that for a fixed draw temperature and speed, the draw stress depends only on the actual draw ratio (R_A) achieved and is independent of the nominal draw ratio (R_N). However, any variation in the draw temperature or draw speed will affect the draw stress because of the associated increase or decrease in the flow stress of the material.

3.3. Structural characterization

3.3.1. WAXS

POM has a hexagonal unit cell with unit cell dimensions of $a = b = 4.45$ Å and $c = 17.3$ Å [20]. The molecular chains are arranged in a 9/5 helix where a and b axes are on the same plane and the chains are aligned parallel to the c axis of the crystal [21]. For POM, the calculated positions of the peaks in the 2θ scan are 22.9°, 34.6°, 48.4° and 54.1° for diffraction planes having Miller indices (100), (105), (115) and (205), respectively [22].

The WAXS patterns of the hydrostatic and die-drawn samples are shown in Fig. 6a and b, respectively. For samples from both processes, the (100) reflection at low draw ratios consisted of a strong maximum on the equator and a weak ring. This suggests that the crystal a axis is preferentially oriented perpendicular to the draw direction with a small portion of isotropic material. At draw ratios greater than 4, the intensity of the weak ring decreased and disappeared completely at R_A of 7 or greater.

Fig. 7a and b shows the 2θ vs. scattering intensity plots from the (100) plane for oriented POM samples produced by hydrostatic extrusion and die-drawing at 160 °C to similar draw ratios. The intensity of the reflections from the (100) plane increased with draw ratio because of the increase in the degree of crystallinity [23,24] and the greater degree of continuity in the alignment of crystals in the draw direction [25].

The orientation of the crystalline phase, f_x, is given by the generalized Hermans' orientation function defined as [26],

$$f_x = \frac{3\langle \cos^2 \phi \rangle - 1}{2} \tag{1}$$

where $\langle \cos^2 \phi \rangle$ gives the average square of the cosine of the angle between the reference crystallographic axis and the chosen reference axis in the sample. For a uniaxially oriented system,

$$\langle \cos^2 \phi \rangle = \frac{\int_0^{\pi/2} I(\phi) \cos^2 \phi \sin \phi \, d\phi}{\int_0^{\pi/2} I(\phi) \sin \phi \, d\phi} \tag{2}$$

where $I(\phi)$ is the relative intensity scattered from the (hkl) plane under consideration. In the case of oriented POM, the reflection from the (100) plane, corresponding to the a axis, can be used to calculate the crystalline orientation factor of

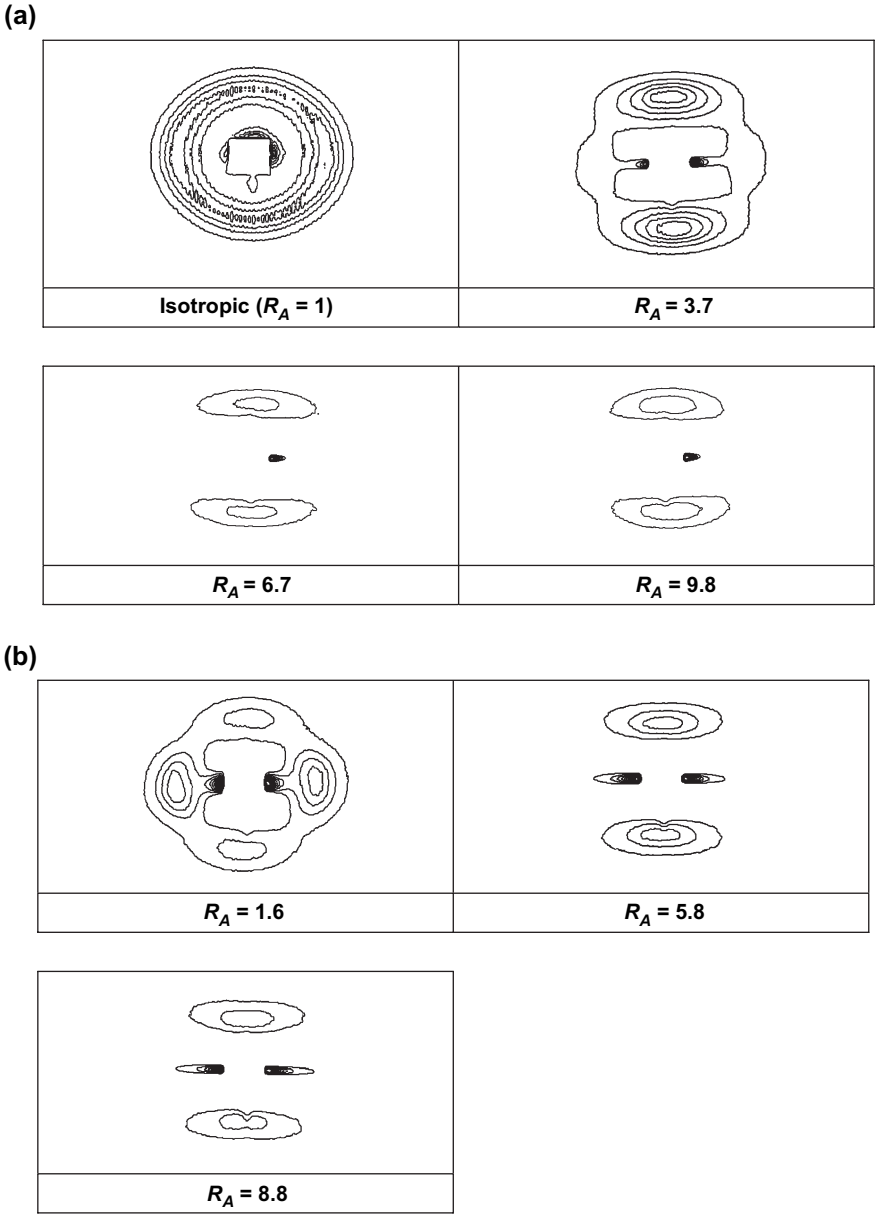

Fig. 9. SAXS patterns at different draw ratios for (a) hydrostatically extruded and (b) die-drawn POM.

the a axis, f_a [22,27,28]. Due to the hexagonal unit cell structure and uniaxial symmetry, the orientations of the a and the b crystallographic axes are equal ($f_a = f_b$). Since

$$2f_a + f_c = 0 \tag{3}$$

the crystalline orientation factor, f_c, can be determined by an azimuthal scan of the (100) plane (2θ fixed at 22.9°).

The effect of draw ratio on the crystalline orientation factor for both the hydrostatic extruded and die-drawn samples measured by this approach is shown in Fig. 8. The crystalline orientation was similar for both processes and appeared almost complete at a draw ratio of around 4. Similar results were reported for a variety of grades of POM oriented by different processing routes [11,15,28,29].

3.3.2. SAXS

The SAXS patterns on the hydrostatically extruded and die-drawn POM samples at different draw ratios are shown in Fig. 9a and b along with the patterns from the isotropic sample which showed a broad isotropic ring with no intensity variation.

The SAXS pattern from the hydrostatic extruded sample of $R_A = 3.7$ and greater draw ratio exhibited two-point ellipsoidal patterns along the meridional direction with diffused scattering along the equator. The broad line structure along the meridional direction is indicative of a variation in lamellar orientation [30]. In the hydrostatic extrusion process, though the mean stress state in the material is compressive, the diffused scattering along the equator in the SAXS patterns suggests that voids are still present in the extruded samples. This observation is consistent with Argon's theory for craze formation in glassy

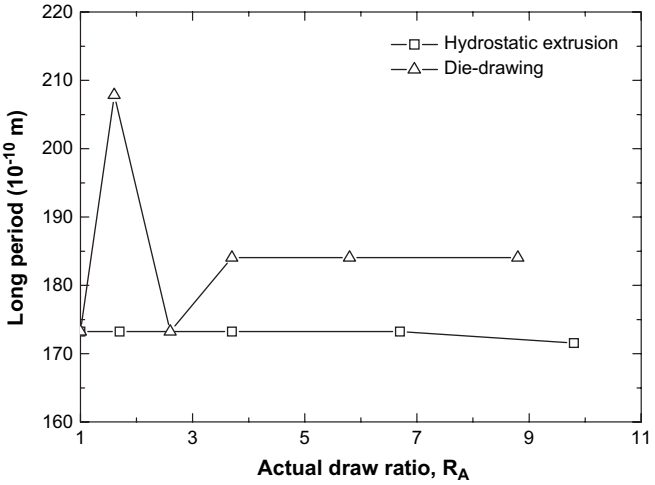

Fig. 10. The variation of long period with draw ratio for hydrostatically extruded and die-drawn POM.

polymers [31]. According to this theory, micro-voids are initiated at stress concentrations by the shear stress during inhomogeneous plastic flow at a molecular level. The growth of the nucleated cavities is due to the tensile principal stresses [32]. In the hydrostatic extrusion process, as the material progresses through the die, it is subjected to shear deformation along the orientation axis that promotes void nucleation. The growth of the nucleated voids is inhibited in the extrusion process due to the absence of a tensile component of stress.

On die-drawing to a R_A of 1.6, the shape of the pattern took an ellipsoidal shape with the long axis perpendicular to the draw direction and a diffused scattering along the equator. Further drawing to a R_A of 5.8 showed a two-point SAXS pattern along the meridian and a broad diffused scattering along the equator. The scattering along the equatorial direction originates from the longitudinal micro-voids formed between the fibrils. Increasing the R_A beyond 5.8 increased the intensity along the equator, suggesting that the micro-void content increased with increasing draw ratio. In a separate series of experiments, the authors have performed a detailed study of the micro-void formation in the die-drawing process and the effect of processing conditions on its nucleation and growth. These results will be published elsewhere.

The long period L was calculated by considering a slice along the meridian of the SAXS pattern from the equation,

$$L = \frac{2\pi}{q^*} \tag{4}$$

where q^* is the scattering vector corresponding to the maxima in the plot of the scattering angle, 2θ and normalized intensity defined by,

$$q^* = \frac{4\pi \sin\theta}{\lambda} \tag{5}$$

where λ is the wavelength of the incident X-ray beam.

The long period of the die-drawn and extruded POM samples as a function of draw ratio is shown in Fig. 10 along with that for the isotropic sample ($R_A = 1$). In the case of the hydrostatically extruded POM, the long period at all draw ratios remained similar to that of the isotropic material.

In the case of die-drawing at low draw ratios, the axial long period increased with R_A. This is thought to be due to the affine displacement of the initial spherulitic structure causing the spacing between the lamellae to increase with plastic deformation. Increasing the R_A to 2.6 causes an abrupt fall in the long period to a value similar to that of the isotropic material. On further drawing to draw ratios greater than 3.6, the long period remained constant. This trend suggests that, at low R_A, the increase in long period is due to the concurrent increase in the spacing of the original lamellae and is dependent on the long period of the start-up (isotropic) material. However, the constant long period at higher draw ratios suggests the formation of a new fibrillar structure caused by the fracturing of the original chain folded lamellar into small blocks, which are restacked into the newly formed micro-fibrils connected by inter-lamellar tie molecules. It has been shown previously by Perterlin and co-workers [30,33], that the new long period is determined only by the temperature of the drawing process and is independent of the long period of the isotropic material. The difference in long period between the die-drawn and hydrostatically extruded samples at higher draw ratios could be possibly due to small differences in the actual temperature of the process, which is affected by the heat generated due to the destruction of the lamellae and plastic work as well as frictional heating.

3.4. Thermal properties

The %crystallinity was calculated from the heat of fusion from the DSC endotherms and was found to increase with draw ratio for both processes as shown in Fig. 11. The heat of fusion of POM crystal was assumed to be 317.93 J/g [34]. The crystallinity of the samples from the hydrostatic extrusion process was higher than for the die-drawn samples at all draw ratios.

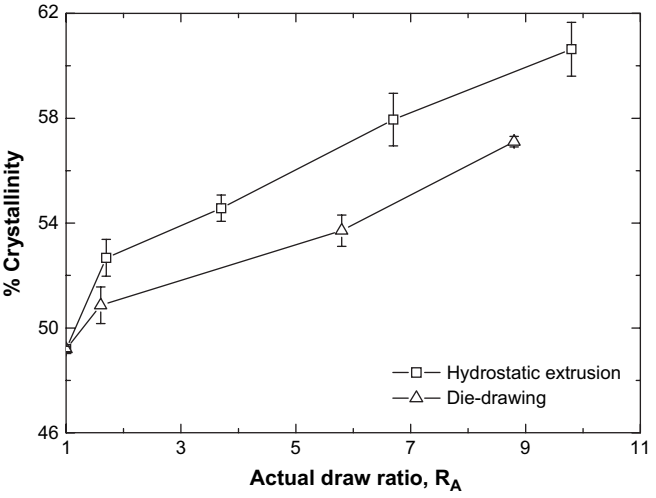

Fig. 11. The variation of %crystallinity with draw ratio for hydrostatically extruded and die-drawn POM.

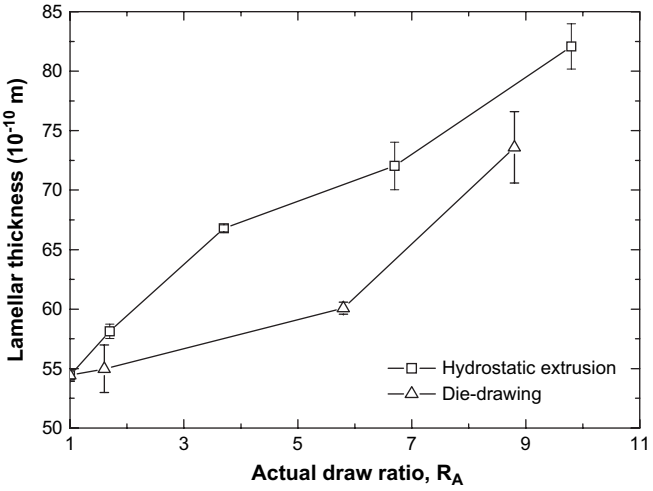

Fig. 12. The variation of lamellar thickness for hydrostatically extruded and die-drawn POM.

From the DSC endotherms, the lamellar thicknesses l of the samples were calculated using the general Gibbs–Thomson equation [35],

$$T_m = T_m^o\left(1 - \frac{2\sigma_e}{\Delta h_o l}\right) \quad (6)$$

Here T_m^o and Δh_o are the equilibrium melting temperature and thermodynamic enthalpy of fusion per unit volume of the crystalline phase, respectively, and σ_e is the free surface energy of the end faces lamellar that is associated with the crystallization process. The values of T_m^o, Δh_o and σ_e for POM assumed in the above equation for calculating the lamellar thickness were 200 °C [36], 380×10^6 J/m^3 [37] and 0.125 J/m^2 [38], respectively. The predicted variation in lamellar thickness with draw ratio is shown in Fig. 12. At all draw ratios considered in this work, the lamellar thicknesses of the hydrostatically extruded products were greater than for the die-drawn samples.

3.5. Morphology

SEM micrographs of the isotropic and oriented samples from both processes are shown in Fig. 13a and b. Isotropic POM exhibited small porosities of the order of few microns dispersed throughout the sample. This is indicative of the fact that in the absence of nucleating agent in the material voiding occurs between the spherulites during the melt extrusion process [39,40].

SEM micrographs of the hydrostatically extruded and die-drawn samples reveal that the spherical porosities, that were present in the start-up material, become elongated along the draw direction. The morphological features of the oriented samples from both the processes appear similar. In the hydrostatic extrusion process, although the material is under a compressive stress field as it progresses through the die, the voids are not physically closed but become extended along the draw direction. In the die-drawing process, the mean stress state of

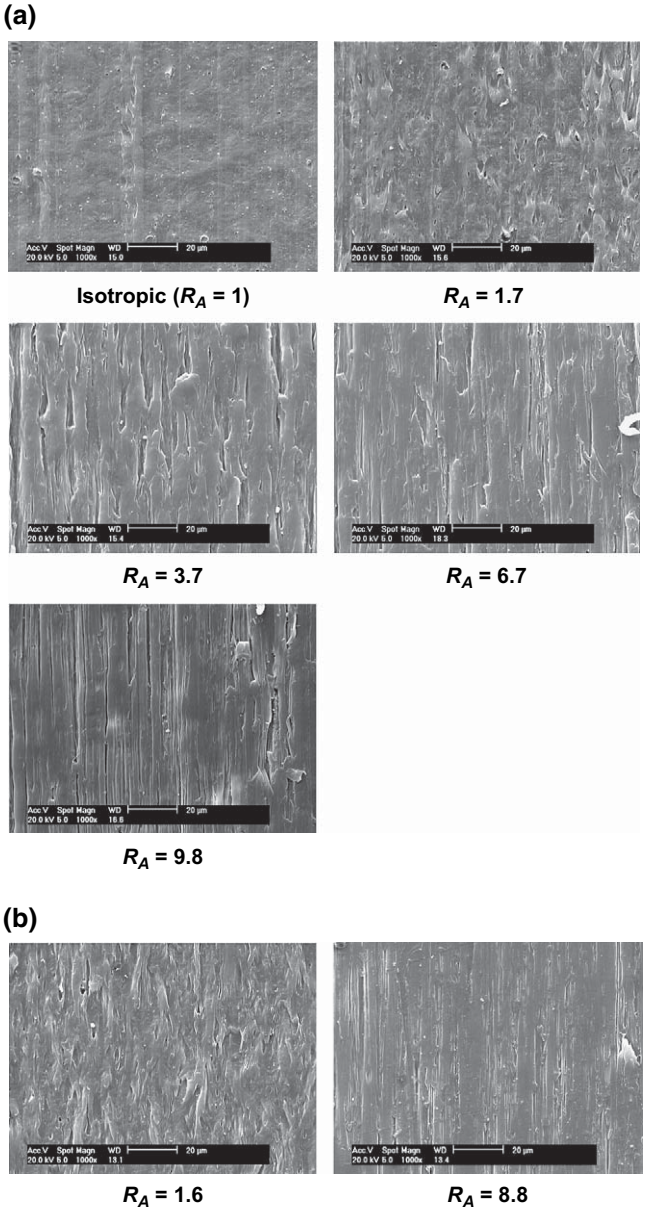

Fig. 13. SEM micrographs at different draw ratios for (a) hydrostatically extruded and (b) die-drawn samples.

the material at the die-exit is tensile, which causes the pre-existing voids to become stretched along the draw direction. It is to be noted that the die-drawing process for the present study was carried out at relatively low speeds to minimize tensile free drawing outside the die. At higher drawing speeds, more voids could nucleate and coalesce causing fibrillation of the material and ultimately leading to fracture when attempting high processing speeds. In an associated paper it will be shown that the extent of voiding in the die-drawing process is a function of the nominal draw ratio, die geometry and the draw speed.

Image analysis was performed on the micrographs using the Image-pro Plus software (Media Cybernetics Inc.) to extract information about the size of the voids. The aspect ratio of the voids, which is defined as the ratio of the major and the

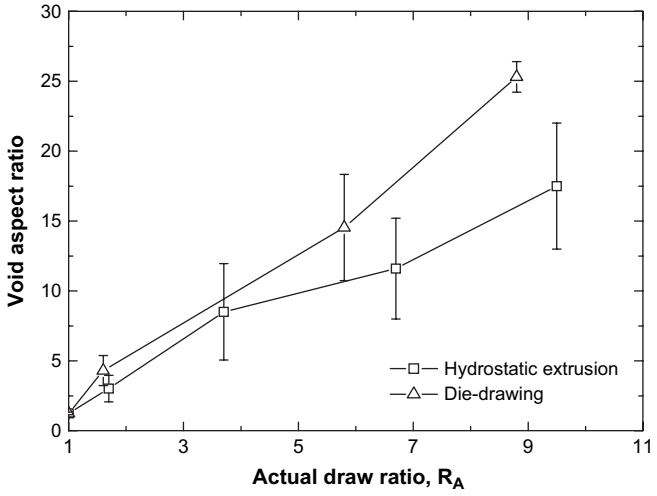

Fig. 14. The void aspect ratio as a function of draw ratio for hydrostatically extruded die-drawn POM.

minor axis, for both processes is shown in Fig. 14. The porosities in the isotropic material were nearly spherical as indicated by the value of aspect ratio close to 1. For both processes, the aspect ratio of the voids increases almost linearly with draw ratio. The void aspect ratio of the die-drawn samples is greater than the extruded samples owing to the tensile nature of the stresses in the former.

3.6. Physical and mechanical properties

3.6.1. Density

Fig. 15 shows the apparent density vs. actual draw ratio for oriented POM produced by hydrostatic extrusion and die-drawing processes. In general, the density of the oriented samples from both the processes decreased with R_A, the rate of decrease in the latter case being higher. The photographs of the oriented samples, machined to a 2 mm thick rectangular strip in the transverse direction from the core of the cylindrical rods, are shown in Fig. 16. A dark line in the background is

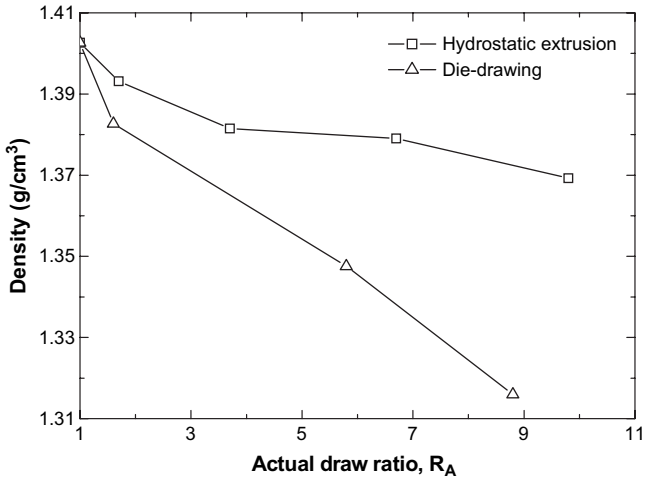

Fig. 15. The effect of draw ratio on the density for hydrostatically extruded and die-drawn samples.

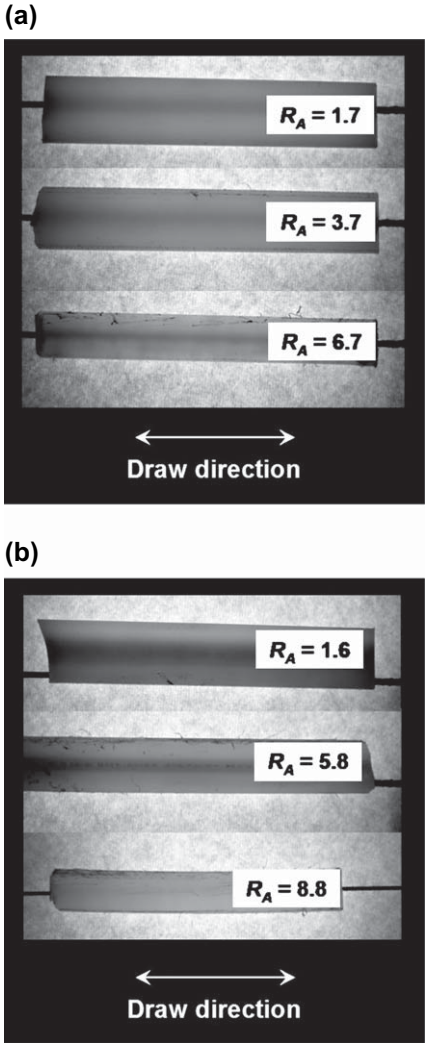

Fig. 16. Photographs of the oriented samples from (a) hydrostatic extrusion and (b) die-drawing processes. The samples were machined to a 2 mm thick rectangular strip from the core of the cylindrical rods.

used as a reference to reveal the opacity of the oriented samples. In the case of the die-drawn samples, a white core was visible in core of the oriented rods due to voiding and hence the reference line is positioned between the core and the surface. It is evident from the photographs that the die-drawn samples are more opaque than the hydrostatically extruded samples for similar draw ratios. The opacity of the die-drawn samples is as a result of voiding due to the tensile nature of the stresses of the material in the die. In an associated paper, the authors have analyzed the extent of voiding in the die-drawn samples as a function of draw speed, reduction ratio (R_N) and post-die cooling conditions. For the samples produced by the hydrostatic extrusion process, as a result of the compressive stress field in the die, the extent of voiding is minimized compared to the die-drawn samples.

3.6.2. Modulus and strength

Fig. 17 shows the effect of draw ratio on the tensile modulus of hydrostatic extruded and die-drawn POM samples

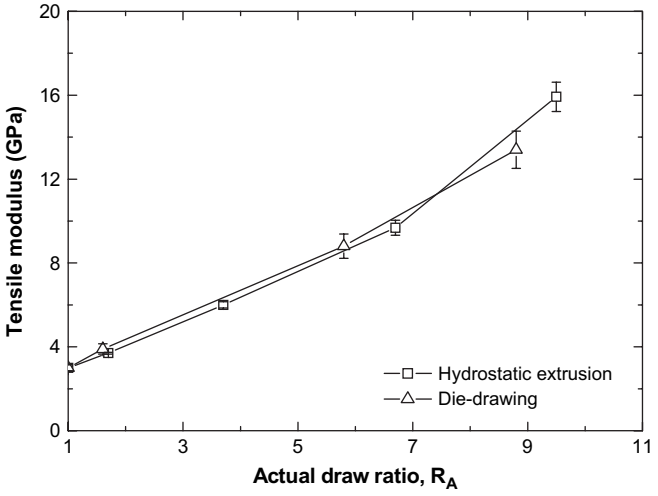

Fig. 17. The effect of draw ratio on the tensile modulus for hydrostatically extruded and die-drawn POM.

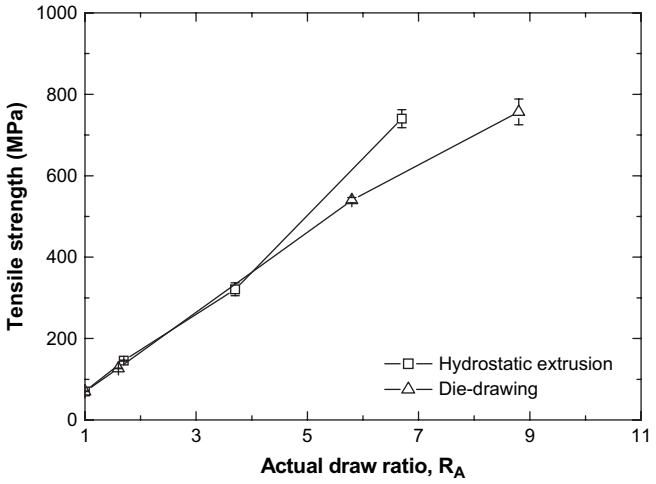

Fig. 18. The effect of draw ratio on the tensile strength for hydrostatically extruded and die-drawn POM.

measured parallel to the draw direction. In both cases, the modulus increased almost linearly with draw ratio. The moduli are within error identical for the two processes. The enhancement in modulus of the drawn sample has been interpreted in terms of the morphology of the drawn sample [24]. According to Peterlin [41], the micro-fibrils are composed of alternating chain folded crystalline blocks connected by taut tie molecules. Taraiya et al. [24] concluded that both the taut tie molecules and extended chain crystals contributed to the improved properties along the draw direction. WAXS studies on samples from both processes suggested that the crystalline orientation is almost complete at a draw ratio of around 6. At higher draw ratios, the improvement in the properties is attributed predominantly to an increasing contribution from the tie molecules. This plot shows that, for a particular polymer grade and draw temperature, the modulus is dependent only on the draw ratio and is independent of the particular orientation process.

The tensile strength vs. draw ratio of the drawn rods measured parallel to the draw direction is shown in Fig. 18. In the case of the die-drawn samples, the strength seems to increase linearly with draw ratio initially and then start to level off at higher draw ratios. Since the crystalline orientation is complete at R_A of around 6, any enhancement in the properties arises from the taut tie molecules formed in the inter-fibrillar and intra-fibrillar regions of the oriented polymer. In the case of the hydrostatic extruded samples, the strength increased approximately linearly with R_A. The strengths of the die-drawn and hydrostatically extruded samples were similar up to R_A of around 4. At higher draw ratios, the samples from the hydrostatic extrusion process were stronger than the die-drawn samples. Attempts to measure the tensile strength of the hydrostatic extruded samples of $R_A = 9.8$ were unsuccessful with sample repeatedly slipping at the grips. It can, however, be speculated from this observation that the hydrostatic extruded sample at this R_A was much stronger than the die-drawn sample. The difference in strength could be due to the higher extent of voiding in the die-drawn samples at higher draw ratios (Fig. 16) producing voids which act as stress raisers to reduce the strength. The lower extent of voiding in the hydrostatic extruded samples, as confirmed by the density measurements means that the strength continues to increase with draw ratio.

4. Conclusions

In this paper we have compared the mechanical properties and physical structure of oriented polyoxymethylene (POM) produced by two processes, die-drawing and hydrostatic extrusion, in which the stresses in the material in the die are predominantly tensile and compressive in nature, respectively. The crystalline orientation and tensile modulus of the oriented POM from both processes at similar draw ratios were very similar, but the strengths were different at higher draw ratios. The fact that the strength of the hydrostatically extruded samples was higher than that of the die-drawn samples can be attributed to the higher extent of voiding present in the die-drawn samples as detected by the SAXS studies and density measurements. The long period of the two samples was also different which could possibly be due to small differences in the actual temperature of the processes. The lamellar thicknesses as determined from the DSC endotherms showed that the hydrostatic extruded samples have thicker lamellae than the die-drawn samples. SEM micrographs revealed that the pre-existing voids in the start-up material are oriented along the draw direction for both process, the void aspect ratio increasing with actual draw ratio.

Acknowledgements

The financial support of this work by the Engineering and Physical Sciences Research Council (Grant no: GR/R80087/01) is gratefully acknowledged. The authors are also grateful to Mr. D. Stephenson, Mr. A.M. Wiese and late Mr. P.E. Hector for their assistance in sample preparation.

References

[1] Gibson AG, Ward IM, Cole BN, Parsons B. Journal of Materials Science 1974;9(7):1193–6.
[2] Zachariades AE, Porter RS. Journal of Macromolecular Science, Physics 1981;B19(3):377–86.
[3] Ward IM. Advances in Polymer Science 1985;70:1–70.
[4] Komatsu T, Enoki S, Aoshima A. Polymer 1991;32(11):1983–7.
[5] Ajji A, Dumoulin MM, Cole KC. Engineering Plastics 1996;9(3):216–24.
[6] Bartczak Z, Morawiec J, Galeski A. Journal of Applied Polymer Science 2002;86(6):1413–25.
[7] Capaccio G, Ward IM. United Kingdom patent specification: 1498628, United Kingdom; 1973.
[8] Clark ES, Scott LS. Polymer Engineering and Science 1974;14(10):682–6.
[9] Brew B, Ward IM. Polymer 1978;19(11):1338–44.
[10] Coates PD, Ward IM. Journal of Polymer Science Part B – Polymer Physics 1978;16(11):2031–47.
[11] Zihlif AM. Materials Chemistry and Physics 1985;13(1):21–45.
[12] Komatsu T, Enoki S, Aoshima A. Polymer 1991;32(16):2992–4.
[13] Komatsu T, Enoki S, Aoshima A. Polymer 1991;32(11):1994–9.
[14] Takeuchi Y, Yamamoto F, Konaka T, Nakagawa K. Journal of Polymer Science Part B – Polymer Physics 1986;24(5):1067–77.
[15] Taraiya AK, Mirza MS, Mohanraj J, Barton DC, Ward IM. Journal of Applied Polymer Science 2003;88(5):1268–78.
[16] Mohanraj J, Bonner MJ, Barton DC, Ward IM. In: Proceedings of 21st polymer processing society conference, Leipzig 2005.
[17] Sahari JB, Parsons B, Ward IM. Journal of Materials Science 1985;20(1):346–54.
[18] Hope PS, Richardson A, Ward IM. Polymer Engineering and Science 1982;22(5):307–13.
[19] Hope PS, Ward IM. Journal of Materials Science 1981;16(6):1511–21.
[20] Carazzolo GA. Journal of Polymer Science Part A: General Papers 1963;1(5):1573.
[21] Tadokoro H, Yasumoto T, Murashashi S, Nitta J. Journal of Polymer Science 1960;44(143):266–9.
[22] Schweizer T, Vancso G. Angewandte Makromolekulare Chemie 1989;173:85–100.
[23] Maeda Y, Nakayama K, Kanetsuna H. Polymer Journal 1982;14(8):649–58.
[24] Taraiya AK, Unwin AP, Ward IM. Journal of Polymer Science Part B – Polymer Physics 1988;26(4):817–38.
[25] Gibson AG, Davies GR, Ward IM. Polymer 1978;19(6):683–93.
[26] Alexander LE. X-ray diffraction methods in polymer science. Chichester: Wiley-Interscience; 1969.
[27] Takeuchi Y, Yamamoto F, Nakagawa K, Yamakawa S. Journal of Polymer Science Part B – Polymer Physics 1985;23(6):1193–200.
[28] Komatsu T, Enoki S, Aoshima A. Polymer 1991;32(11):1988–93.
[29] Kaito A, Nakayama K, Kanetsuna H. Journal of Applied Polymer Science 1986;32(2):3499–513.
[30] Balta-Calleja FJ, Peterlin A. Journal of Materials Science 1969;4(8):722–9.
[31] Argon AS, Hannoosh JG. Philosophical Magazine 1977;36(5):1195–216.
[32] Argon AS, Salama MM. Philosophical Magazine 1977;36(5):1217–34.
[33] Peterlin A, Sakaoku K. Journal of Applied Physics 1967;38(11):4152.
[34] Iguchi M. Die Makromolekulare Chemie 1976;177(2):549–66.
[35] Wunderlich B. Macromolecular physics. New York: Academic; 1980.
[36] Salaris F, Turturro A, Bianchi U, Martuscelli E. Polymer 1978;19(10):1163–70.
[37] Brandrup J, Immergut EH. Polymer handbook. 3rd ed. New York: Wiley; 1989.
[38] Plummer CJG, Menu P, Cudremauroux N, Kausch HH. Journal of Applied Polymer Science 1995;55(3):489–500.
[39] Nowacki R, Kolasinska J, Piorkowska E. Journal of Applied Polymer Science 2001;79(13):2439–48.
[40] Galeski A, Piorkowska E. Negative pressure development during crystallization of polymers. In: Imre AR, Maris HJ, Williams PR, editors. Liquids under negative pressure, vol. 84. London: Kluwer Academic; 2002. p. 127–36.
[41] Peterlin A. Journal of Materials Science 1971;6(6):490–508.